Journal Pre-proofs

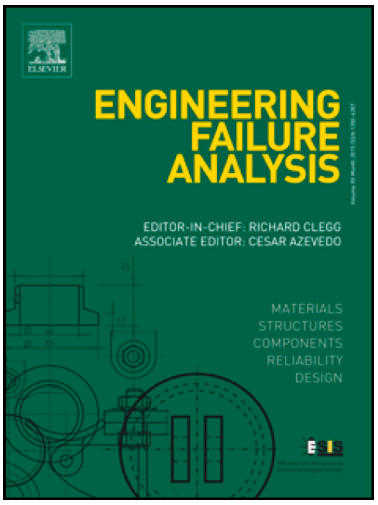

Assessment of unusual failure in crankshaft of heavy-duty truck engine

Karim Aliakbari, Reza Masoudi Nejad, Sayed Kian Pourhosseini Toroq, Wojciech Macek, Ricardo Branco

PII: S1350-6307(22)00059-0
DOI: https://doi.org/10.1016/j.engfailanal.2022.106085
Reference: EFA 106085

To appear in: *Engineering Failure Analysis*

Received Date: 4 December 2021
Revised Date: 18 January 2022
Accepted Date: 20 January 2022

Please cite this article as: Aliakbari, K., Masoudi Nejad, R., Kian Pourhosseini Toroq, S., Macek, W., Branco, R., Assessment of unusual failure in crankshaft of heavy-duty truck engine, *Engineering Failure Analysis* (2022), doi: https://doi.org/10.1016/j.engfailanal.2022.106085

Assessment of unusual failure in crankshaft of heavy-duty truck engine

Karim Aliakbari[a,*,karim-aliakbari@tvu.ac.ir], Reza Masoudi Nejad[b], Sayed Kian Pourhosseini Toroq[a], Wojciech Macek[c], Ricardo Branco[d]

[a]Department of Mechanical Engineering, Technical and Vocational University (TVU), Tehran, Iran

[b]School of Mechanical and Electrical Engineering, University of Electronic Science and Technology of China, Chengdu, 611731, PR China

[c]Gdansk University of Technology, Faculty of Mechanical Engineering and Ship Technology, 11/12 Gabriela Narutowicza, Gda´nsk 80-233, Poland

[d]University of Coimbra, CEMMPRE, Department of Mechanical Engineering, Coimbra, Portugal

*Corresponding author.

Highlights

- The unusual premature failure of a heavy-duty truck engine crankshaft has been investigated.
- The failure was happened to begin with the growth of the fatigue crack from the surface defects.
- The stress analysis was performed on the crankshaft.
- The analysis of fractographic and metallographic was performed on the failed crankshafts.
- Numerical stress analysis has predicted that the highest stress agreed with the fracture zone.

Abstract

The unusual premature failure of a heavy-duty truck engine crankshaft has been the subject of a rigorous study, and this manuscript describes it in detail. The failure was happened to begin with the growth of the crack from the surface defects, in the form of the clusters of non-metallic inclusions, in the lubrication hole zone of the first main journal, which was the stress concentration zone. A series of experiments including chemical composition, microstructure, mechanical properties, hardness, toughness, and fractography were performed on the failed crankshaft. In addition, the stress analysis was performed on the crankshaft. Careful

fractographic study with scanning electron microscopy equipped with energy dispersive spectroscopy revealed that failure with cluster inclusions MnS ($r = {}^{S}/_{Mn} = 0 \cdot 024 > 0 \cdot 01$) was more than the standard amount. Besides, stress analysis showed that the stress field in stress concentration zones with the lubricating hole is much less than the web-crankpin fillet but the presence of cluster impurities, low hardness (> 600 HV0.1 proposed standard), downshifting has caused the growth of primary cracks. It is recommended to first increase the hardness by about 43% and then, decrease the size of non-metallic inclusions so that primary crack growth does not initiate from the worst clusters of inclusions.

Keywords: Diesel engine; Crankshaft failure; MnS inclusions; Downshifting; Microstructure.

1. Introduction

The crankshaft is the most important rotary part of the engine that translates the linear motion of the piston into rotational motion. Crankshaft failures may be induced by several causes, and mechanical fatigue failures are probably the most common cause of crankshaft failures. Also, crankshafts rotate with a stable torsion combined with rotatory bending load and fatigue is the main failure mode [1, 2]. Injuries resulting from the crankshaft damage contain not only the crankshaft itself but also other engine components including the connecting rods, bearings, pistons, and the cylinder block is affected by the crankshaft failure. Therefore, failure analysis plays an essential role in preventing similar failure events and design improvement, manufacturing techniques, and so on [3, 4]. Since the crankshaft failure, as an important part of engines, is a significant subject for engineers, a large number of crankshafts have been failed based on the crankshaft misalignment, inappropriate geometry, insufficient oil, improper design, incomplete assembly, crankshaft imbalance, and incorrect heat treatment process mostly contribute for the fatigue failure of crankshaft [5, 6]. The phenomenon of the fatigue crack growth (FCG) in engineering component has become one of the most important issues [7-12]. Xu and Yu [13] investigated the failure analysis of truck diesel engine crankshaft after 13656 km of service. Fatigue cracks in the sixth, fifth and fourth crankpins were initiated at machining dents present on the wall of the oil hole. The appearance of the machining dents on the wall of the oil hole suggests improper machining and these dents supplied the stress concentration site that was mainly responsible for the fatigue fracture of the crankshaft. Wang et al. [14] investigated failure analysis of crankshaft via theoretical calculation, finite element modeling, and fractographic observation in fracturing pumps. The results indicated that fatigue fracture was the dominant failure mechanism, with evidence of beachmarks, striation marks,

and multiple fatigue cracks. Also, the main cause of insufficient fatigue strength was the absence of surface hardening treatment. Besides, the fillet radius was the main factor for fatigue crack initiation, the fatigue cracks were mostly located in the thread root of radial oil-hole. Their finite element analysis results indicated that the stress increased remarkably as the fillet radius decreased. Wang et al. [15] evaluated the analysis of an unusual crankshaft failure after only 20 min. Experimental tests revealed that four cracks were found on the edge of the oil hole due to the force of friction caused by improper crankshaft repair and assembling. Font et al. [16] investigated the failure mode analysis of two crankshafts of a single-cylinder diesel engine after 100 hr of service. Results clearly showed that fatigue was the dominant mechanism of failure for both crankshafts: one fatigue crack was initiated at crankpin-web fillet and the other one into the end of the large oil bore. Also, numerical results showed stress at the inner main oil bore zone less than the crankpin fillet zone. But the SEM micrographs of crack initiation inner the lubricating oil bore of the crankpin revealed that the drilling grooves can act as micro notches due to high-stress concentration.

Most studies of crankshafts failure analysis have referred to fatigue crack growth from the web-crankpin zone due to high-stress concentration points. Fewer failures have happened in the main journal of the crankshaft and therefore, fewer articles have been published due to failure analysis of the main journal. In the crankshaft case study, failure has occurred in the lubricating oil hole of the main journal. In summary, the novelties and objectives of the present work can be stated as follows:

- Selecting a novel case study of unusual premature failure of crankshaft.
- Preparing experimental measurements on failure analysis including mechanical properties (hardness, Charpy toughness, and tensile tests), the chemical composition of the material.
- Imaging material microstructure using an optical microscope (OM) and fractography of fracture surface using a scanning electron microscope (SEM).
- Analyzing harmful nonmetallic inclusions using energy-dispersive spectrometry (EDS).
- Analyzing the stress field in the stress concentration zones.
- Investigating the failure causes and finding the root cause of the failure from the main journal zone.

2. Case study reports

In this research, a crankshaft of the heavy-duty truck engine failed at operation within 600000 km of service from the lubricating hole zone of the first main journal that the features of this engine are shown in Table 1. Also, Figure 1 indicates the fracture location of the crankshaft from the lubricating hole zone of the first main journal.

The geometric dimensions were measured with the Micrometer and Vernier Caliper of the Mitutoyo Corporation of Japan. The accuracy of the Micrometer and the Vernier Caliper was 0.01 mm and 0.05 mm, respectively. Macroscopic observations were done using a Samsung 8MP AF camera with a 1.22 μm pixel size. The chemical composition of the crankshaft material was examined according to ASTM E415-14 [17] standard and ASTM E1086-14 [18] standard by SPECTROMAXx manufactured in Germany. To conduct the hardness and microstructure, a cross-section of the main journal with a thickness of 8 mm was cut by the wire-cut EDM machine and was treated using successive abrasive SiC papers, and fine polishing is used by diamond and silica suspensions. Washing in alcohol and drying in hot air were used as the final step of finishing. Microstructure revealing, immersion etching was performed using an aqueous solution of Nital 2% (solution of 2% v/v HNO_3 in ethanol) according to [19, 20]. Then, optical microscopies (OM), as well as scanning electron microscopy (SEM) along with energy dispersive spectroscopy (EDS) were carried out to characterize the microstructure and fractography. EDS examination of the sample cross-section was examined in order to characterize inclusions. Finally, the hardness test was performed using a hardness measurement device under 500 gr applied force for 10 seconds according to ASTM E384-11e1 [21] standard and Ref [22]. For evaluating the mechanical properties of the crankshaft material, such as ultimate stress (σ_{US}), yield stress (σ_{YS}), and elongation, the three samples were machined by a CNC lathe as shown in Figure 2. The samples were then tested in accordance with the ASTM E8/E8M-15a [23] standard and Refs [24, 25]. The results of the experiment were stored at the sampling rate of 2 times per second in the form of force-displacement. The length variation of the specimens was measured by an extensometer with a length of 50 mm. In order to perform the test, the displacement speed of the machine grips was set at 0.50 mm.min^{-1}.

For fractography examination, first, the fractured surface section from the main journal of the failed crankshaft was cut by an EDM machine and then the sample was placed in an ultrasonic bath for one hour and finally, images were made with high magnifications by SEM machine

model LEO 1450VP having EDS model 7335. Also, EDS was able to measure the chemical composition of the base material and impurities inside and around the crack zone. To determine the Charpy toughness, standard Charpy specimens were first machined from the fractured crankshaft location and the experiments were performed at room temperature. At least four specimens as shown in Figure 3 were tested to obtain the Charpy V-notch energy.

3. Results and Discussions

3.1. Chemical Composition Analysis

The average results of the crankshaft material chemical composition are listed based on weight percent in Table 2. The values of the determining elements in Table 2 are equal to 38MnVS6 / DIN 1.1303 in the DIN EN 10083-3:2007-01 [26] standard. 38MnVS6 steel is a common Manganese–Vanadium alloy steel according to DIN standard, and 1.1303 steel is under W-Nr Germany standard. The use of DIN 1.1303 steel is recommended for automotive components like crankshafts, pushrods, rotating bearings, axle journals, hubs, and piston heads. This high-strength Mn-V-based steel is a low alloy high-grade steel with good machinability for controlled cooling from working heat.

3.2. Material Properties of Crankshaft

The mechanical properties of the crankshaft material compared to the applicable standard specifications are listed in Table 3. The first row of Table 3 shows the average values of the three examined samples. Figure 4 shows the diagram of the tensile test at 24 °C (ambient temperature). Also, the value obtained from the tensile test at ambient temperature is within the equivalent standard characteristics to steel DIN 1.1303 / 38MnVS6.

3.3. Microscopic Examination

Figure 5-a shows the macrograph of the specimen cross-section of the main journal by the camera and also Figure 5-b to 5-d shows the micrograph of the specimen cross-section of the main journal by OM. The macrostructure at the cross-section of the main journal reveals a case-hardened layer as the component was subjected to induction hardening treatment (Figure 5-a). The hardening layer was uniform along the cross-section and its thickness specification was about 8 mm. The un-etched microstructure reveals numerous inclusions throughout the specimen which indicates that the steel is not clean (Figure 5-b). Figure 5-c and Figure 5-d

show the layers of the hardened edge-core and core hardened, respectively, the larger the grains as they move towards the core of the sample.

3.4. Hardness Investigation

Uniform distribution of hardness with low slope is observed in the main journal sample across the section (Figure 6). The average hardness of the surface hardened layer was measured to be 420 HV which is acceptable compared to the core hardness of 276 HV. The ratio of surface hardened layer to core hardness is desirable since it imparts ductility. But, according to the technical standard, the hardness of the quenched layer should be more than 600 HV0.1, which was less than the technical requirements [5, 6, 15]. On the other hand, in the present study, uniform hardness distribution is considered an advantage because the non-uniform distribution of hardness with a great slope as axle shaft in [27] was caused by brittleness.

3.5. Evaluation of Charpy Toughness

A test is required to determine the behavior of materials when are subjected to high rates of loading (the impact resistance or toughness), usually in bending, tension, or torsion. The quantity measured is the energy absorbed in breaking the specimen by a single blow, as in the Charpy (simple-beam) test or the Izod (cantilever-beam) test according to ASTM E23−12c [28] standard. It was not possible to conduct Charpy toughness tests with the dimension of 10×10 mm on the failed crankshaft location due to the limitation of material. The ASTM Method for Notched Bar Impact Testing of Metallic Materials (E23−12c) [28] allows the use of sub-size specimens (with the dimension of 5×5 mm) when the amount of material available does not permit making the standard impact test specimens. These sub-sizes were estimated to produce errors < 0.1 J [29]. The Charpy V-notch energy was found to be as follows: Maximum Charpy Energy=0.95 kg-m, Minimum Charpy Energy=0.8 kg-m. In general, the specimens fractured parallel to the notch plane present a ductile fracture appearance (Figure 7). The fracture appearance resulting from the impact test of this material at ambient temperature is similar to the test performed in [30] that has a good agreement to the amount of hardness obtained, the microstructure of the material, and surface fracture of the failed crankshaft.

3.6. Fractography of Fracture Surface

The primary purpose of fractography science is finding the origin of the crack and it is necessary for a proper analysis of the fracture. Initiation and propagation of the cracks would create distinctive signs on the fracture surface, such as river signs, radial lines, chevrons, and

beachmarks that indicate the growth direction of the cracks. These marks are examined for finding the origin of the cracks. The appearance of these marks on the fracture surface is a function of tensile loading type, shearing, bending, fatigue or torsional; stress state; stress amount; stress concentration existence; environmental factors and material factors [31-33]. Visual inspection indicates that the fracture surface is rough and represents a very complicated ratchet or diagonal lines pattern and the sides of the ratchet marks are at approximately ±45° angle to the crankshaft axis, similar to the typical fracture of torsional failure [34-37]. The ratchet marks were generated when cracks were collected at different circumferential points and were linked together creating ridges on the fracture surface [38]. The existence of ratchet marks also indicated multiple origins and high-stress concentration [39]. Figure 8 indicates fracture location and surface of the crankshaft that the fracture surfaces were heavily damaged by scratching. Before the engine was disassembled at the repair shop, the crankshaft was separated into two parts, reported by the technician at the repair shop. Hence, the scratching marks with identical clockwise-anticlockwise directions on the fracture surface cannot be generated either during the disassembling or the transportation of the fractured crankshaft. Figure 8-a shows the fracture site of the lubricating oil hole in the unbroken crankshaft, which rarely fails in this zone. Figure 8-b shows the presence of thick coverings and the severe damage on the fracture surfaces that were removed to analyze from the fracture surface.

The local plastic deformation directions at the scratching locations on the fracture surface can be determined according to the scratch marks. The plastic deformation directions at the scratching locations on the fracture surface were all clockwise-anticlockwise (turning-downshifting directions) as shown by two-way yellow arrows in Figure 8-c. The term downshifting in automotive engineering refers to the act of speed reduction (high torque multiplication) while driving with high speed a vehicle with manual transmission. On the other hand, the direction of plastic deformation at the scratching locations on the fracture surfaces was all clockwise (turning direction) as shown in [5]. Unlike the predominant fracture mode, where crack growth (see red arrows) propagates from the outer surface of the part to the part core, in the failed crankshaft, the direction of crack growth from the inner surface of the oil channel to the outer surface of the part is due to excessive dimples (see green circles) and cluster impurities. The cluster impurities are shown in metallographic images (Figure 5-b). The cracks initiation from the inner surface of the oil channel and propagated to the outer surface of the crankshaft, as mentioned in [13], which originated from cracks due to machining dents. In addition, the red arrows indicate the predominant direction of crack growth, which has deviated slightly when reaching the hardened layer of the cyan dashed line (Figure 8-c). The

original fracture surface was observed by SEM to analyze the micro-fractographic features. As shown in Figure 9, the presence of dimples in SEM images taken from the core of the fracture surface with less hardness indicates ductile fracture. It was indicated that the crankshaft underwent reversed cyclic torsional loading (downshifting) in its service. Similar failures were occurred due to reversed cyclic torsional loading in the spline-shaft of an under-slung crane [36] and truck diesel engine crankshaft [5] as the Refs.

3.7. SEM and EDS

Due to the unusual premature failure of the crankshaft and the presence of the inclusions in Figure 5-b, imaging of the etched material by SEM with high magnification is required to investigate inclusions precision size and hardened layer size, and their role in the failure analysis. On the other hand, EDS was used to measure the chemical composition of inclusions.

As a result of the role of the inclusions in the material strength, the percentage of inclusions in the present study was investigated using MIP software as shown in Figure 10-a. Also, Figure 10-b indicates some inclusions on the matrix with high magnification. The percentage of inclusions was measured to be about 2.4% and if the percentage is greater than 0.01% in a 1% Mn steel (see Table 4), it forms a series of clusters that can also act as the initiation of cracks.

Figure 11-a and Figure 11-b display the size of one inclusion and its EDS spectra, respectively. The EDS spectra of the steel reveal the composition of the inclusions as shown in Figure 11-b. Through the EDS data analysis, it was verified that the inclusions are mainly composed in a large amount by manganese and sulfur, possible due to manganese sulfide (MnS) precipitation, a common (but not desirable) phenomenon that occurs during the cooling process of low carbon steels, and affects the mechanical properties, failure, and fatigue of steel parts. The existence of these inclusions according to Ref [40] is detrimental to both the surface quality and the forming properties of the final products. Moreover, the existence of sharp inclusions can cause stress concentration, which in turn causes cracks to grow due to the cyclic load.

3.8. FEM analysis

First, for stress field analyses, the full crankshaft with true profile geometry has been constrained to build the finite element model. All other parameters such as material properties, boundary conditions, meshing, and methods for the model are defined according to [41-43]. Tetrahedral elements were chosen to execute the crankshaft mesh that is convenient for

complex geometries. The finite element model consists of a total of 134172 elements. In order to do stress analysis in crankshaft structure, some data are needed to identify including Young modulus (E), Poisson's ratio (υ), and Yield stress. These parameters are specified as the input of software modeling and analysis. Mechanical properties of crankshaft steel are defined in Table 3. Figure 12 shows the stress field due to the loading of crankshaft analysis. For the crankshaft, the maximum magnitude of von Mises stress appears to be 89.84 MPa after loading in the stress concentration zone of the web-crankpin fillet. Besides, stress analysis showed that the stress amount of 18.3 MPa in the stress concentration zone of the lubricating hole is much less than the web-crankpin fillet but the presence of cluster impurities, downshifting, and low hardness has caused the growth of the cracks.

Table 5 shows the solution of the problem in terms of the number of elements and the maximum von Mises stress for the crankshaft according to Refs [44, 45]. As can be seen, the most appropriate number of elements is 134172 elements for the crankshaft that the maximum von Mises stress created in the crankshaft is equal to 89.84 MPa, as shown in Figure 12. This means that a proper convergence has been created between the stress 89.84 MPa and the number of elements 134172.

4. Failure Causes Investigation

Figure 11 clearly shows the fact that the increase of manganese sulfide (MnS) precipitation is considerable in the material matrix. Not only, the existence of these inclusions according to Refs. [46, 47] are harmful to both the surface quality and forming properties of the final products, but also, reversed cyclic torsional loading (downshifting) in its service and the high-stress concentration at the main journal lubricating hole zone, lead to initiation and propagation of cracks. On the other hand, the FEM results of the complete crankshaft model [16, 41, 43, 48] and the one crank model [41, 49] showed that the fillets of crankpin–web according to Figure 12 were the most vulnerable part and this, in turn, causes the crack initiation and propagation. However, in this study, the crack was initiated in the lubricating hole zone of the main journal, which rarely occurs in this zone. Wakoh et al. [50] proved that the reason for the formation of MnS nucleation is due to when the sulfur content is higher than 0.01% in a 1% Mn steel. According to [50, 51], if the sulfur content is higher than 0.01% in a 1% Mn steel, it will form MnS nucleation. In this article, the ratio of S to Mn ($r = S/Mn = 0 \cdot 036/1 \cdot 51 = 0 \cdot 024 > 0 \cdot 01$) is very higher than 0.01. Due to the ratio of S to Mn being about 2.4 times, therefore this high amount increases the possibility of MnS formation as inclusions clusters.

The results of this observation by EDS prove this theory showing that inclusions of MnS are not distributed evenly on the steel background and in some places lead to the formation of the microcracks clusters. The percentage of measured inclusions is about 2.4% using the above calculation and MPI software as clusters series of inclusions plus downshifting can act as initiation and propagation of crack fastly, respectively.

5. Conclusion

The study of considering crankshaft failure in service after 600,000 km of operation of the six-cylinder heavy-duty truck diesel engine was conducted, and the following results were drawn.

1. OM and chemical composition results showed that the steel microstructure is a kind of low carbon alloyed steel composed of ferrite (α) and perlite (P) phases in which MnS nonmetallic inclusions are frequently seen in the cross-section area of the test sample having the average size of around 4 μm.

2. Obtained results from tensile test indicted the mechanical properties of the crankshaft material compared to the applicable standard specifications are acceptable and the equivalent is with standard characteristics to steel DIN 1.1303 / 38MnVS6.

3. The uniform distribution of hardness with a low slope is observed in the main journal sample across the section. The average hardness of the surface hardened layer is measured to be 402 HV which is acceptable compared to the core hardness of 276 HV and also for these applications. But, according to the technical standard, the hardness of the quenched layer should be more than 600 HV0.1, which was less than the technical requirements.

4. The morphology of the fracture surface shows that the crankshaft has been failed due to the growth of cracks caused by cluster impurities in the lubrication hole zone. Reverse torsional loading (downshifting) and stress concentration in the lubrication hole zone has been accelerated the ductile failure.

5. Unlike the predominant fracture mode, where crack growth propagates from the outer surface of the part to the part core, in the failed crankshaft, the direction of crack growth from the inner surface of the oil channel to the outer surface of the part is due to excessive dimples and cluster impurities. In addition, the diagonal lines pattern on the fracture surface indicates the predominant direction of crack growth, which has deviated slightly when reaching the hardened layer.

6. The results of this observation by EDS prove this theory showing that inclusions of MnS are not distributed evenly on the steel background and in some places lead to the formation of the microcracks clusters. The ratio of S to Mn is very higher than 0.01 and the percentage of

measured inclusions is about 2.4% using calculation and MPI software as clusters series of inclusions plus downshifting can act as initiation and propagation of crack fastly, respectively.

Acknowledgments

The authors would like to appreciate the sincere cooperation of Mr. M. Esfidani (Materials Mechanical Properties Lab, Ferdowsi University of Mashhad) and Mr. D. Khademi (Electron Microscopy Research Core, FUM Central Lab).

References

[1] K. Aliakbari, Failure analysis of four-cylinder diesel engine crankshaft, J. Brazilian Soc. Mech. Sci. Eng. 41 (2018) 30.

[2] Y. Tominaga, J. Kim, Y. Pyun, R. Kayumov, J. Kim, J. Woo, A study on the restoration method of friction, wear and fatigue performance of remanufactured crankshaft, J. Mech. Sci. Technol. 27 (2013) 3047–3051.

[3] M. Fonte, V. Anes, P. Duarte, L. Reis, M. Freitas, Crankshaft failure analysis of a boxer diesel motor, Eng. Fail. Anal. 56 (2015) 109–115.

[4] K. Aliakbari, N. Safarzadeh, S.S. Mortazavi, Analysis of the crankshaft failure of wheel loader diesel engine, Int. J. Eng. Trans. B Appl. 31 (2018).

[5] X. Xu, Z. Yu, Failure analysis of a truck diesel engine crankshaft, Eng. Fail. Anal. 92 (2018) 84–94.

[6] V. Infante, J.M. Silva, M.A.R. Silvestre, R. Baptista, Failure of a crankshaft of an aeroengine: A contribution for an accident investigation, Eng. Fail. Anal. 35 (2013) 286–293.

[7] Nejad, Reza Masoudi, Mohammadreza Tohidi, Ahmad Jalayerian Darbandi, Amin Saber, and Mahmoud Shariati. "Experimental and numerical investigation of fatigue crack growth behavior and optimizing fatigue life of riveted joints in Al-alloy 2024 plates." Theoretical and Applied Fracture Mechanics 108 (2020): 102669.

[8] Shariati, Mahmoud, Majid Mirzaei, and Reza Masoudi Nejad. "An applied method for fatigue life assessment of engineering components using rigid-insert crack closure model." Engineering Fracture Mechanics 204 (2018): 421-433.

[9] Nejad, Reza Masoudi. "The effects of periodic overloads on fatigue crack growth in a pearlitic Grade 900A steel used in railway applications." Engineering Failure Analysis 115 (2020): 104687.

[10] Nejad, Reza Masoudi. "Numerical study on rolling contact fatigue in rail steel under the influence of periodic overload." Engineering Failure Analysis 115 (2020): 104624.

[11] Nejad, Reza Masoudi, Zhiliang Liu, Wenchen Ma, and Filippo Berto. "Fatigue reliability assessment of a pearlitic Grade 900A rail steel subjected to multiple cracks." Engineering Failure Analysis 128 (2021): 105625.

[12] Nejad, Reza Masoudi, Zhiliang Liu, Wenchen Ma, and Filippo Berto. "Reliability analysis of fatigue crack growth for rail steel under variable amplitude service loading conditions and wear." International Journal of Fatigue 152 (2021): 106450.

[13] X. Xu, Z. Yu, Failure Analysis of a Truck Diesel Engine Crankshaft Made from Spheroidal Cast Iron, J. Fail. Anal. Prev. 11 (2011) 332–336.

[14] H. Wang, S. Yang, L. Han, H. Fan, Q. Jiang, Failure analysis of crankshaft of fracturing pump, Eng. Fail. Anal. 109 (2020) 104378.

[15] C. Wang, C. Zhao, D. Wang, Analysis of an unusual crankshaft failure, Eng. Fail. Anal. 12 (2005) 465–473.

[16] M. Fonte, P. Duarte, L. Reis, M. Freitas, V. Infante, Failure mode analysis of two crankshafts of a single cylinder diesel engine, Eng. Fail. Anal. 56 (2015) 185–193.

[17] ASTM E415 - 17, Standard Test Method for Analysis of Carbon and Low-Alloy Steel by Spark Atomic Emission Spectrometry, ASTM International, Philadelphia, 2017.

[18] ASTM E1086 - 14, Standard Test Method for Analysis of Austenitic Stainless Steel by Spark Atomic Emission Spectrometry, ASTM International, West Conshohocken, PA, 2014.

[19] W. Harris, K. Birkitt, Analysis of the failure of an offshore compressor crankshaft, Case Stud. Eng. Fail. Anal. 7 (2016) 50–55.

[20] Z. Siemiątkowski, T. Szumiata, M. Gzik-Szumiata, R. Martynowski, M. Rucki, Application of the microscopic and Mössbauer studies to the analysis of a marine diesel engine crankshaft, J. Mar. Eng. Technol. 17 (2018) 160–167.

[21] ASTM E384 - 17, Standard Test Method for Microindentation Hardness of Materials, ASTM International, West Conshohocken, PA, 2017.

[22] K. Aliakbari, Failure Analysis of Base Plate Bolts of Radial Forging Machine, J. Stress Anal. 4 (2019) 89–98.

[23] ASTM E8 / E8M - 16ae1, Standard Test Methods for Tension Testing of Metallic Materials, ASTM International, West Conshohocken, PA, 2016.

[24] K. Aliakbari, K. Farhangdoost, Plastic deformation influence on material properties of autofrettaged tubes used in diesel engines injection system, J. Press. Vessel Technol. Trans. ASME. 136 (2014).

[25] K. Aliakbari, the investigation of modelling material behavior in autofrettaged tubes made from aluminium alloys, Int. J. Eng. 27 (2014) 803–810.

[26] D.I.N.E.N. 10083-3: 2007-01, Steels for Quenching and Tempering—Part 3: Technical Delivery Conditions for Alloy Steels, German Version EN 10083-3: 2006.(2007) ,
[27] S. Das, G. Mukhopadhyay, S. Bhattacharyya, Failure analysis of axle shaft of a fork lift, Case Stud. Eng. Fail. Anal. 3 (2015) 46–51.
[28] A. E23-12c, Standard Test Methods for Notched Bar Impact Testing of Metallic Materials, ASTM International, West Conshohocken, PA, 2012.
[29] N.H. Fahey, Effects of Variables in Charpy Impact Testing., WATERTOWN ARSENAL LABS MA, 1962.
[30] J. Chao, R. Rementeria, M. Aranda, C. Capdevila, J.L. Gonzalez-Carrasco, Comparison of ductile-to-brittle transition behavior in two similar ferritic oxide dispersion strengthened alloys, Materials (Basel). 9 (2016) 637.
[31] K. Aliakbari, Failure Analysis of Ductile Iron Crankshaft in Four-Cylinder Diesel Engine, Int. J. Met. (2021).
[32] ASM Handbook Volume 13B, American Society for Metals, Metals Park, OH, 2010.
[33] M.R. Torshizian, K. Aliakbari, M. Ghonchegi, Failure Analysis of Ductile Iron Differential Housing Spline in 4WD Passenger Car, Int. J. Met. 15 (2021) 587–601.
[34] H.E. Boyer, H.E. Boyer, Metal Hanbook, Failure Analysis and Prevention, American Society for metals, 1975.
[35] M. Haghshenas, W. Savich, A case study on fatigue failure of a transmission gearbox input shaft, J. Fail. Anal. Prev. 17 (2017) 1119–1125.
[36] P. Sinha, S. Bhattacharyya, Failure investigation of spline-shaft of an under slung crane, J. Fail. Anal. Prev. 13 (2013) 601–606.
[37] S.F. Hassan, M.R. Alam, Failure analysis of gearbox and clutch shaft from a marine engine, J. Fail. Anal. Prev. 10 (2010) 393–398.
[38] G. Pantazopoulos, S. Zormalia, A. Vazdirvanidis, Investigation of fatigue failure of roll shafts in a tube manufacturing line, J. Fail. Anal. Prev. 10 (2010) 358–362.
[39] N.W. Sachs, Understanding the surface features of fatigue fractures: how they describe the failure cause and the failure history, J. Fail. Anal. Prev. 5 (2005) 11–15.
[40] K. Aliakbari, T. Akbarpour Mamaghani, Analysis of fatigue crack growth in cylinder head bolts of gasoline engine based on experimental data, J. Brazilian Soc. Mech. Sci. Eng. 42 (2020).
[41] K. Alilakbari, M. Imanparast, R. Masoudi Nejad, Microstructure and fatigue fracture mechanism for a heavy-duty truck diesel engine crankshaft, Sci. Iran. 26 (2019) 3313–3324.

[42] K. Aliakbari, R. Masoudi Nejad, T. Akbarpour Mamaghani, P. Pouryamout, H. Rahimi Asiabaraki, Failure analysis of ductile iron crankshaft in compact pickup truck diesel engine, Structures. 36 (2022) 482–492.

[43] J. Mateus, V. Anes, I. Galvão, L. Reis, Failure mode analysis of a 1.9 turbo diesel engine crankshaft, Eng. Fail. Anal. 101 (2019) 394–406.

[44] K. Aliakbari, S. Kamel Abbasnia, R. Masoudi Nejad, M. Manoochehri, Analysis of stress intensity factors in railway wheel under the influence of stress field due to heat treatment and press-fitting process, Eng. Fail. Anal. (2021) 105736.

[45] R. Masoudi Nejad, P. Noroozian Rizi, M.S. Zoei, K. Aliakbari, H. Ghasemi, Failure Analysis of a Working Roll Under the Influence of the Stress Field Due to Hot Rolling Process, J. Fail. Anal. Prev. (2021).

[46] J.H. Park, D.S. Kim, Effect of CaO-Al 2 O 3-MgO slags on the formation of MgO-Al 2 O 3 inclusions in ferritic stainless steel, Metall. Mater. Trans. B. 36 (2005) 495–502.

[47] Y. Tanaka, F. Pahlevani, S.-C. Moon, R. Dippenaar, V. Sahajwalla, In situ characterisation of MnS precipitation in high carbon steel, Sci. Rep. 9 (2019) 1–12.

[48] F.H. Montazersadgh, A. Fatemi, Dynamic load and stress analysis of a crankshaft, SAE Technical Paper, 2007.

[49] I. Elishakoff, C.M. Fu, C. Jiang, B.Y. Ni, X. Han, G.S. Chen, Comparison of uncertainty analyses for crankshaft applications, ASCE-ASME J. Risk Uncertain. Eng. Syst. Part B Mech. Eng. 1 (2015) 41002.

[50] M. Wakoh, T. Sawai, S. Mizoguchi, Effect of S content on the MnS precipitation in steel with oxide nuclei, ISIJ Int. 36 (1996) 1014–1021.

[51] S. Lyu, X. Ma, M. Chen, Z. Huang, Z. Yao, G. Wang, B. Zhao, Application of phase equilibrium studies of CaO-SiO2-Al2O3-MgO system for oxide inclusions in Si-deoxidized steels, Calphad. 68 (2020) 101721.

Figure 1. Terminology and fracture location of the crankshaft; (a) Terminology, (b) Fracture surface, and (c) Fracture location.

Figure 2. Samples of tension test; (a) Extracting the standard sample from the engine crankshaft, and (b) The standard samples after the test were done.

Figure 3. Dimensions of Charpy V-notch specimen (in mm).

Figure 4. Engineering stress according to engineering strain curve of crankshaft material.

Figure 5. Macrostructure and microstructure of the cross-section of the failed crankshaft material; (a) Macrostructure of the cross-section; (b) Un-etched microstructure structure; (c) Microstructure of the edge of the component; (d) Microstructure of the core of the component.

Figure 6. Hardness distribution from outer surface toward the center of the main journal in the crankshaft.

Figure 7. Results of Charpy test; (a) measured Charpy V-notch energy, (b) and (c) fracture surface of Charpy sample with magnification of 65X and 110X.

Figure 8. Fracture location and surface of the crankshaft: (a) Fracture location of without fractured main journal, (b) Fracture location from lubricating oil hole, and (c) Fractured surface of the crankshaft.

Figure 9. The presence of dimples in the core of the fracture surface.

Figure 10. Images of SEM; (a) Using MIP with 250X magnification, and (b) with 500X magnification

Figure 11. Spectrum of fracture surface to find impurity particle; (a) SEM image, (b) EDS spectrum.

Figure 12. Stress distribution of von Mises; (a) In complete crankshaft, and (b) In crankpin in detail.

Table 1. Engine specifications and conditions.

1	Engine configuration	4 stroke- cycle, diesel

2	Displacement (cc)	8700
3	Bore × Stroke (mm)	117 × 135
4	Max Power (kW/rpm)	250 / 1800-2100
5	Max. Torque (Kgm/rpm)	132 / 1000-1750
6	Fuel system	High pressure common rail
7	No. of cylinder	6 in-line
8	Firing order	1-5-3-6-2-4
9	Gearbox type	Manual- 12 speed

Table 2. Particulars of failed samples.

Sample type	C	Si	Mn	P	S	Cr	Mo	V	N
Failed crankshaft	0.387	0.53	1.51	0.02	0.036	0.173	0.014	0.104	0.019
Standard alloy	0.34-0.41	0.15-0.8	1.2-1.6	0.025≤	0.02-0.06	0.3≤	0.08≤	0.08-0.2	0.01-0.02

Table 3. Mechanical properties of the failed crankshaft material and standard alloy (38MnVS6).

Specimen type	σ_{YS} (N/mm^2)	σ_{US} (N/mm^2)	Fracture elongation (%)
Failed crankshaft	616.382	902.67	13.00
38MnVS6	min. 520	800-950	min. 12

Table 4. Microstructure Specifications of the material Used in crankshaft.

Sample	Nodularity (%)	Inclusions (%)	Base material (%)
Failed crankshaft	70.07	≥ 2.4	≤ 97.6

Table 5. Results of FE modelling for different element number for crankshaft.

Step	number of crankshaft elements	Maximum von-Mises stress (MPa)
1	100247	98.78
2	108887	93.25
3	110273	90.97
4	123495	89.51
5	134172	89.84
6	146706	90.33